Analysis of the Gas Entrainment by Vortex in the Upper Plenum of the ASTRID Reactor Mock-up

D. Guenadou, P. Aubert, J.-P. Descamps

▶ **To cite this version:**

Analysis of the Gas Entrainment by Vortex in the Upper Plenum of the ASTRID Reactor Mock-up

David Guenadou, Philippe Aubert, Jean-Philippe Descamps
Commissariat à l'Energie Atomique et aux Energies Alternatives
Centre de Cadarache, 13115 Saint Paul lez Durance, France
david.guenadou@cea.fr, phillipe.aubert@cea.fr, jean-philippe.descamps@cea.fr

ABSTRACT

The 4th generation sodium fast neutron reactor ASTRID (Advanced Sodium Technological Reactor for Industrial Demonstration) is developed by the CEA and several industrial partners. The design is in progress especially for the vessel and the equipment. From the state of art of the former sodium reactors PHENIX and SUPER-PHENIX and the EFR program (European Fast Reactor) the global and the local thermal-hydraulic issues have been listed. But the results of those previous projects are not sufficient for the current ASTRID development. New needs for experimental means were identified, especially for both validation of numerical codes and specific studies. In this way, a thermal-hydraulic loop, the PLATEAU facility, was developed and built at the CEA Cadarache research center in 2012. Since experiments with sodium are complex to carry out due to the harmfulness of this liquid metal, the tests are led in models using water as simulant fluid. Different mock-ups can be connected to this loop to study the different issues at various reactor conditions. The first model connected to the PLATEAU facility is MICAS, mock-up of the hot plenum. This one is dedicated to study the flow regime, both for code validation and engineering design development. It was designed at 1/6 scale and was built in transparent polymer to carry out optical measurements as laser velocimetry and fast imaging.

Gas entrainment by vortex is one of the issues identified and can have an impact on the vessel design. Gas occurrence in the core induces neutron effects which may leadto core reactivity variation. Gas entrainment was first investigated at the MICAS free surface using fast imaging. A tendency regarding the geometry and the operating parameters was identified. Further investigations were focused on the velocity field around the vortices in the way to develop a gas entrainment criterion. Two types of vortex occur at the free surface: those which induce gas entrainment, and those which do not. By the used of the Burgers vortex model, the downward velocity gradient and the circulation are identified as parameters influencing the gas entrainment. From the tangential velocity measured by particles image velocimetry around various types of vortex, the downward velocity gradient and the circulation were calculated using the Burgers model. Results showed that the Burgers model fit the experimental tangential velocity. Depending on the gas entrainment occurrence among the different studied vortex, a value for the gas entrainment criterion was found.

KEYWORDS

Vortex, mock-up, sodium fast reactor, particle imaging velocity

1. INTRODUCTION

Nuclear energy can play an important role to provide sustainable and carbon-free electricity. However, the current Gen II and Gen III reactor types use fuels only composed by the uranium 235 isotope which accounts for a very low part (0.71%) of the raw uranium mineral. The estimate stocks cover reactors operations during about 100 years. The Gen IV reactors intend to use the wide spread uranium 238 isotope (99.28%). In this case, the stocks are estimated for thousands years of operation. Moreover, as the Gen II and Gen III spent fuels are mainly composed by uranium 238, those wastes should be reuse in the Gen IV reactors type in order to close the nuclear fuel cycle. From those advantages, CEA

and many industrial partners are involved in the development of a Gen IV industrial prototype: ASTRID (Advanced Sodium Technological Reactor for Industrial Demonstration) [1].

ASTRID is a pool reactor cooled by sodium. The main advantage of pool type reactor is to maintain the primary sodium in one main vessel. It reduces the risk of primary sodium leakage. The figure 1 is a sketch of the actual design. The sodium flows from the external vessel to the upper plenum through the core where it is heated. As in PHENIX and SUPER-PHENIX, the fuel assemblies are hexagonal shaped and the pin bundle are surrounded by helical wire spacers. Around 90% of the sodium ejected from the core is deviated by the Above Core Structure (UCS) to the upper plenum. The other part flows across the ACS, then to the upper plenum. This structure aims at monitoring the core state by the use of thermo-velocimetry probes above each fuel assembly. The ACS also holds the control rode.The hot sodium (550°C) of the upper plenum enters inside the Intermediate Heat Exchangers (IHX) to heat a secondary sodium circuit. This latter is connected to a steam generator. This scheme avoids the primary sodium to be in contact with water in case of leakage. The outlet of the IHX is connected to the lower plenum where the sodium is pumped and sent back to the core. Detail presentations of ASTRID and the project are given in [1-4].
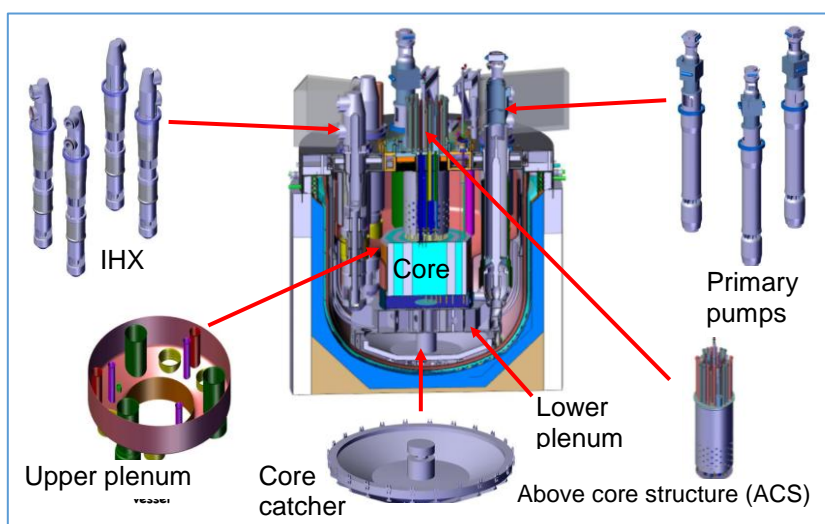

Fig. 1. Cut view of the ASTRID primary circuit.

CEA has a lot of experience in sodium cooled reactors technology [5]. However, due to the improved design of ASTRID compared to the former reactor (PHENIX, SUPER-PHENIX), new experimentations are needed both for studying the design options and for validating the code calculations [6-7]. Experimentations with sodium are very complex due to its opacity and its high reactivity with water. As water and sodium are very close regarding physical properties, in terms of density and viscosity, most experiments are performed with water. In this framework, the PLATEAU loop was built in 2012 [8]. It aims at providing the experimental conditions, in terms of flow rate and temperature, to the various models. The first mock-up, MICAS, commissioned in 2015, represents the upper plenum of the ASTRID reactor at a 1/6 scale [8]. It aims at studying the main thermal-hydraulic issues such as the gas entrainment at the free surface [9].

If a gas pocket was released into the core, a positive reactivity effect would occur and may lead to safety problems. As a consequence, gas accumulation in the diagrid has to be avoided. One of the origins of gas [10-11] is due to the vortices created at the free surface in the upper plenum. An argon blanket covers the sodium to avoid any contact with air and limit the temperature. Gas entrainment may occur at the tip of some vortices by various processes: bubbles may be teared from the gas core tip; a gas column may be sucked into the IHX. To design the upper plenum, it appears crucial to identify the hydraulic conditions creating vortices with gas entrainment. Many studies were carried out to study the behaviour of the vortices and the criteria of gas entrainment [12-16] but most of them were performed in analytical setups and their results can't be applied directly for industrial reactor

design. Previous studies on the MICAS mock-up [9] stated the vortices and gas entrainment occurrence depending on the experimental operating conditions (water head, flow rate, vessel design…). They were helpful to eliminate some design options which lead to high probability of gas entrainment, but useless to draw design guidelines for lessening the vortex occurence. The aim of this study is to find in the ASTRID reactor real geometrical conditions a gas entrainment criterion based on the local velocity at the free surface. It will be used for upper plenum design purposes and CFD validation. In this aim, surface velocity measurements were performed in the MICAS mock-up by the help of the Particle Image Velocity (PIV) technique. The first part of this article is devoted to present briefly the MICAS mock-up and the PIV setup. The second one presents the gas entrainment criterion and the last paragraph is dedicated to the results.

2.   THE MICAS MOCK-UP AND THE PIV SETUP

A top-view of the MICAS mock-up is shown on the figure 2. Its dimensions are about 2.5 m in diameter and 1.7 m in height. A scale of 1/6 the ASTRID reactor was chosen to be a compromise between the overall size and the detail of the geometry of the vessel (such as the ACS), but some geometrical simplifications were necessary. For example, the hexagonal fuel assemblies in the core were replaced by cylindrical tubes. Nevertheless, the IHX are represented in detail owing to the impact of their design on the flow pattern as the fluid is exiting the vessel. Due to its location just above the core, the ACS highly influences the flow pattern; for this reason, its geometry in MICAS is very detailed.

The core is constituted by various types of assembly, such as the fuel assemblies where the fission reactions take place or the neutron shielding assemblies which avoid material activation. Because of the different pressure loss of each type of assembly, the flow distribution in the ASTRID core is quite complex [4]. As it would be difficult to reproduce the exact core flow map in the MICAS mock-up, it was simplified into 3 flow zones. The central zone represents the fission assemblies, and the two surrounding ones are respectively the reflectors and the internal storage.
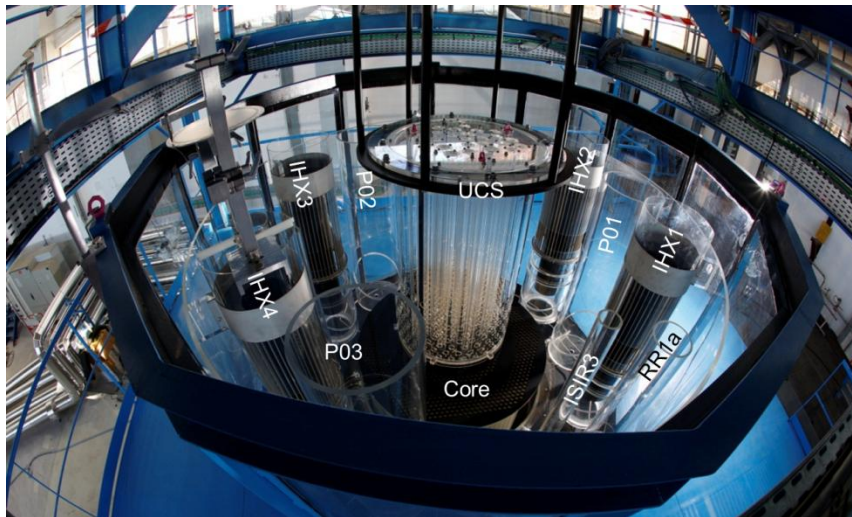

Fig.2. Top view of the MICAS mock-up (P0x stands for the pump pit, UCS, for the Upper core Structure, IHXx, for the Intermediate Heat Exchanger, ISIRx, for the inspection in operation, RRxa, for the decay heat exchanger)

The operating parameters in the MICAS model are calculated using the dimensionless analysis. As our investigations are focused on the gas entrainment and surface state behaviour, Froude number similitude is considered. By assuming the same Froude number in the reactor and mock-up, the flow rate in the MICAS mock-up is expressed by Eq. (1).

$$Q_{MICAS} = Q_{ASTRID} \cdot L^{*2.5} \qquad (1)$$

Where Q_{MICAS} and Q_{ASTRID} are respectively the mock-up and reactor flow-rates, L* the mock-up scale.

Most of the components of the MICAS model are built using a high optical quality grade Polymethyl methacrylate (PMMA) transparent polymer for optical visualizations and PIV measurements. The model is surrounded by a 12 PMMA walls pool filled with water to reduce the optical deformations. As water and PMMA have close refraction index (1.3 and 1.5) compared to air (refraction index≈1), the optical deformations are lessened by the thin water layer between the mock-up and the plane faces of the external pool.

PIV technique is used to measure the surface flow velocity in the MICAS model. This technique allows acquiring 2D large velocity fields. It is based on the measurement of particles displacement during two short laser pulses separated by a brief delay. In our setup, the laser is set on a 3-axis motion table to get as accurate as possible positioning. Large measurement domains are obtained thanks to a laser sheet to enlighten the particles. Clean DI water is used in the MICAS mock-up, but as the free surface is open air, it catches dust and atmospheric particles so that no additional particles were needed in the water. The particles scatter the laser light which is recorded on a 4 Mpixels CCD camera located perpendicular to the laser sheet. A filter at the laser wavelength is set on the camera in order to only get the light scattered by the particles and to avoid the noise due to ambient light. Nevertheless, the ambient light has an influence on the results and to reduce this effect, black curtains are put all around and over the model to be in the darkest possible conditions. Moreover, those curtains were compulsory for laser safety reasons. Calibrations are carried out prior to the measurement using a target. The measurement domain is meshed in cells depending on the amount of particles. The time delay between the two laser pulses is calculated regarding the mean velocity and particles density. A particle should not exit the cells during its motion between the two laser pulses. The knowledge of the approximate mean velocity and the cell size allows calculating the time delay between the two pulses. This parameter is tuned during the experiments regarding the velocity results. Data were analysed using the Insight 4G software (version 10.10.4). For all the experiments, the mesh size was 128x64 with a 15 Hz acquisition rate.

For all the locations investigated, the horizontal laser sheet was created at 20 mm below the free surface. The camera was located over and perpendicular to the water surface. We assumed that the little wavy behaviour of the surface do not alter the recorded images and does not impact significantly the velocity accuracy. As the camera is equipped with a 35mm lens, the measurement domain is quite large: 140 mm X 140 mm.

3.   GAS ENTRAINMENT CRITERION

Sakai and al. [17] suggested modelling the gas entrainment using the Burgers vortex model [18]. This one is expressed by the equations (2)-(4) below:

$$u_r = -\frac{1}{2}\alpha r \tag{2}$$
$$u_z = \alpha z \tag{3}$$
$$u_\theta = \frac{\Gamma}{2\pi r}\left(1 - exp\left(-\frac{r^2}{4(\frac{\nu}{\alpha})}\right)\right) \tag{4}$$

Where u_r, u_z, u_θ are the velocity components of the vortex in the r, z, θ the polar coordinates system, Γ is the circulation, α is the downstream velocity gradient, and ν is the cinematic viscosity.

The gas core length in one of the key parameters that influences the gas entrainment onset. It seems obvious that longer the core is, more gas entrainment occurs. By the other hand, the distance between the vortex tip and the flow outlet plays an import role. If the vortex tip is close to the outlet, bubbles

will be easily entrained. From this state, Sakai and al. [17] suggest a criterion for the gas entrainment based on the water depth and the core length calculated from the Burgers model:

$$\frac{L_{gc}}{h} = \frac{Ln(2)}{16\pi^2}\left(\frac{\alpha\nu}{gh}\right)\left(\frac{\Gamma}{\nu}\right)^2 = K.\alpha^*.\Gamma^{*2} \qquad (5)$$

Where L_{gc} and h are the core length and the outlet depth, g is the gravity acceleration, ν is the cinematic viscosity, K is a constant, α^* and Γ^* are dimensionless parameters.

The equation (5) expresses the competition between the gas core length and the outlet depth. The gas entrainment occurs when the ratio L_{gc}/h in equation (5) reaches one, i.e. when the gas core is as long as the IHX outlet depth. Sakai and al. determined the criterion for gas entrainment by solving t $L_{gc}/h=1$ from the equation (5) [17]. The raw result expresses that when $\alpha^*.\Gamma^{*2}<228$ no gas entrainment occurs; but the authors considered three time allowance to the theoretical model so that they set the criterion for no gas entrainment when $\alpha^*.\Gamma^{*2}<76$. By using velocity around the vortexes in the MICAS upper plenum mock-up, we suggest to determine an experimental criterion and compare it to this theoretical one.

4.   RESULTS

Experiments are carried out in the MICAS mock-up according to the Froude number similarity. In some specific operating conditions, the reactor runs with only 2 IHXs open, the 2 others being closed. In this case, the flow rate is set at 60% of the nominal value. It leads to increase the velocity by 20% at the IHXs inlet as global area is divided by two. This configuration creates huge vortices at the water surface as shown on the figure 3. Two types of vortex appear on the left hand picture of the figure 3. On the right one, air is sucked from the water surface to the IHX inlet and a large amount of gas is carried into the diagrid. The tip of the other one ends close to the IHX inlet and bubbles of air may be entrained in the IHX. Both vortices are not allowed during the reactor operation because of the potentiality of gas entrainment. We have to guaranty that no gas is carried into the diagrid. At the MICAS water surface, from the visualization of vortex carrying gas into the IHX or not, we can build a vortex database in a way to define a gas entrainment criterion using the equation (5). The two parameters α^* and Γ^*can be calculated from the Burgers model in equations (2)-(5) by knowing the experimental velocity field around the vortex. As the vortices are rather stable during the experiment and their location foreseeable, we can measure the velocity field around them by the PIV technic. This will be performed for vortex carrying gas or not.

A raw picture of the PIV measurement is presented in the figure 4. We can recognize the core assemblies exits and the vortex. Because the laser sheet is emitted from the left hand side of the picture, the laser sheet is deteriorated behind the vortex due to the reflexion index changes. The light gets throw two non-plane water/air surfaces. On the figure 4, we can observe particles in the left hand area of the vortex, but none in the right hand side. From this observation, the only left hand side velocity of the vortex is accurate and available.
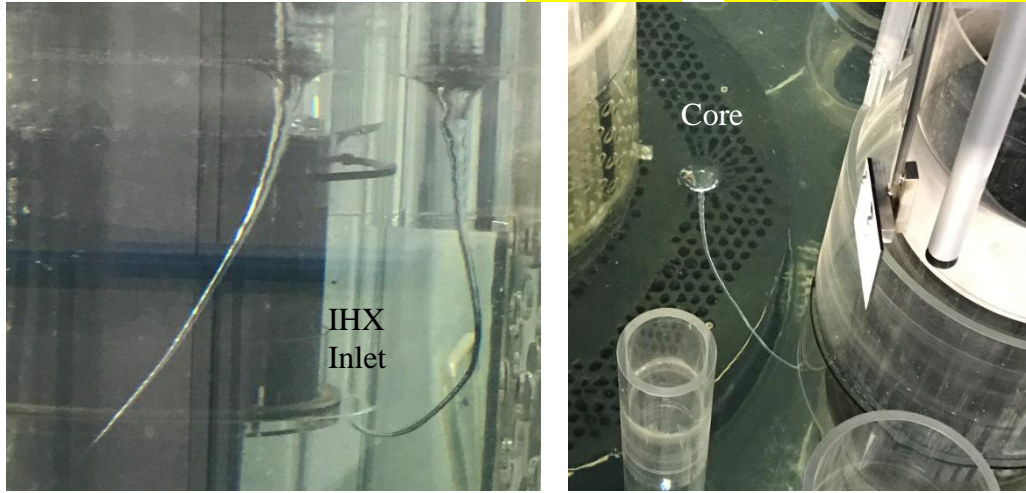
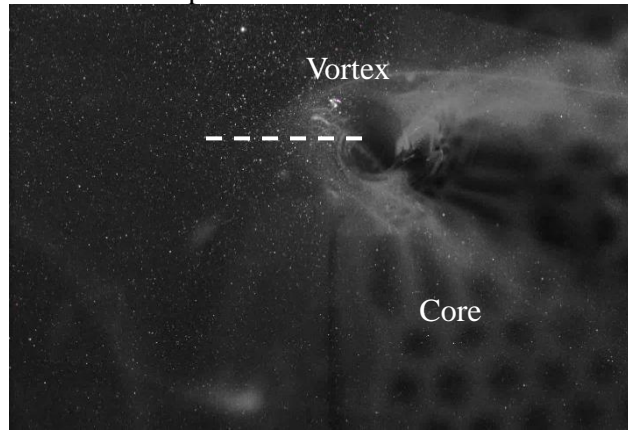Fig. 3. Front and top view of vortices in the MICAS mock-up

Fig. 4: Raw picture for the PIV measurement

The tangential velocity along the dash line on the figure 4 is plot according to the red square curve in the graph of the figure 5. The vortex centre is on the right hand side of the graph at the null radius. In the gas core, the velocity cannot be measured because the air does not contain enough particles to scatter the light. This is the reason why, close to the vortex centre, the measurement velocity is null. We noticed in the figure 5 the velocity increases sharply from the centre core and decreases in the outer vortex region. A top value is reached at about 24 mm from the core centre. At this location, the derivative of the tangential velocity versus the radius is null. By using the derivative of the equation (4), we can express the downward gradient velocity parameter of the Burgers model by the equation (6).

$$-\frac{\alpha}{4\nu}r_m^2 + Ln\left(1 + \frac{\alpha}{2\nu}r_m^2\right) = 0 \tag{6}$$

Where α is the downward velocity gradient, ν is the cinematic viscosity and r_m is radius at the maximal velocity from the vortex centre.

The α parameter is calculated by solving the equation (6) and the Γ parameter is determined using the equation (4) and the velocity at the r_m radius. The Burgers model tangential velocity using those calculated parameters is plotted in blue on the graph of the figure 5. We can notice that the model is close to the experimental results. In the outer vortex region, some discrepancies occur due to the influence of the surface flow.
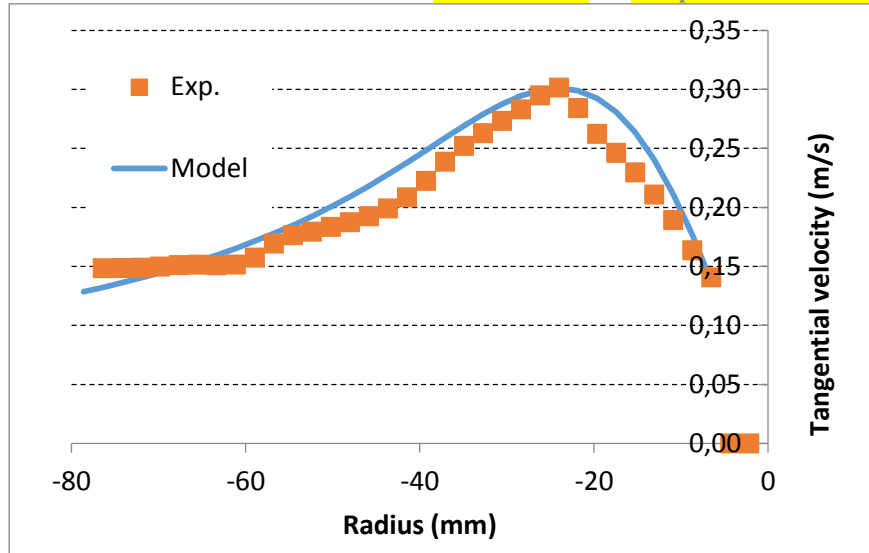
Fig. 5. Experimental and Burgers model tangential velocities versus the vortex radius.

The gas entrainment criterion expresses in the equation (5) only depends on the downward velocity gradient and the circulation. From the results obtained during the experimental campaign on the MICAS mock-up, a downward velocity and circulation database has been built. For each PIV velocity measurement around the vortex, the circulation and the downward velocity gradient are determined by the method presented in the former paragraph. The graph in the figure 6 shows the downward velocity gradient (α) versus the circulation (Γ) depending on gas entrainment occurrence for each vortex investigated during the MICAS experimental campaign. At first, we can notice in the figure 6 that at low circulation values, the vortices do not entrain gas. But the circulation is not the only criteria determining the air entrainment onset; in the circulation range of 30-60, we observe both none and gas entrainment. The downward velocity gradient also plays a role in the air entrainment phenomenology. But its impact seems lower than the circulation since high downward velocity gradients do not generate gas entrainment. This fact appears in the equation (5), the gas entrainment criterion depends on the square of the circulation but it is only proportional to the downward velocity gradient. This finding may be useful to reduce the gas entrainment by acting on the upper vessel design to lessen the circulation. As this one is promoted by the wake of the immerged components, the IHX outlets should be located as far as possible from them. The surface flow velocity also plays an important role on the circulation and could be simply decreased by enlarging the vessel size.

The bar graph of the figure 7 presents the gas entrainment criterion based on the works of Sakai and al. [17] and applied to the results of the MICAS experimental campaign. It was calculated from the equation (5) using the circulation and the downward velocity gradient database determined previously. The blue bars show the values for the vortices which entrain gas and the red ones refer to no entrainment. We remark that the air entrainment occurs when the criterion reaches high values. Below a given value, the gas is still not entrained. This is consistent with the statement of the equation (5) which expresses the ratio of the core length over the distance to the outlet. Higher is this ratio, bigger is the probability of gas entrainment. From the results of the figure 7, we can state that the criterion for the air entrainment onset is in the range of 4 to 5. In the green area of this graph, no vortex entrains gas below the value of 4, but gas entrainment occurs for all vortices over the value of 5. We can set the experimental gas entrainment criterion $\alpha^*.\Gamma^{*2}<4$. We can notice that this one is smaller by a ratio 50 compared to the theoretical one calculated by Sakai and al. [17]. This difference may be due to the fact that the turbulence is not taken into account in the Burger model. The geometry also may influence the gas entrainment criterion, especially the IHX outlet design. In many analytical experiments [14-16], the vortex is created by sucking the water using a vertical tube. In the MICAS mock-up, the fluid gets out horizontally through the IHX. Further investigations are in progress to understand the discrepancies between the experimental and theoretical criterion values.
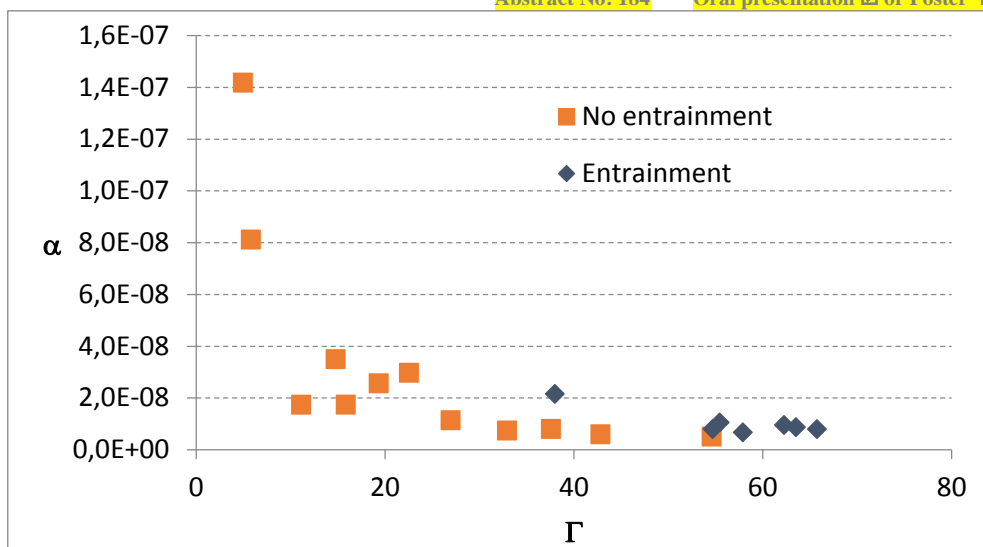
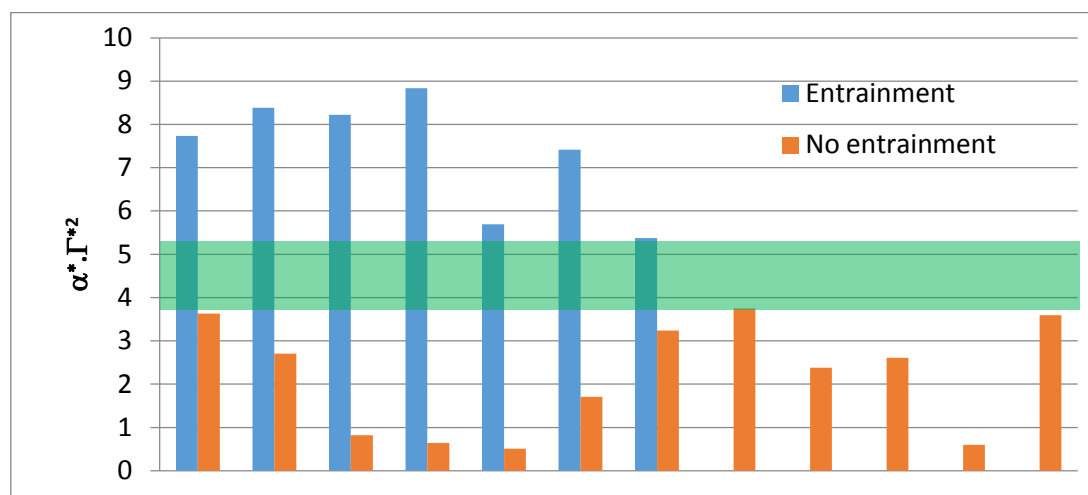Fig. 6. Downward velocity gradient (α) versus circulation (Γ) depending on gas entrainment occurrence.

Fig. 7. Gas entrainment criterion depending on the type of vortex.

4. CONCLUSION

The 1/6th scaled MICAS mock-up is dedicated to study the flow behaviour in the upper plenum of the ASTRID reactor. The first studies were carried out with the same Froude number regarding the reactor and the model to get similar surface flow behaviour. As gas entrainment by vortex is one of the major thermal hydraulic issues in the upper plenum of the ASTRID reactor, one main aim of the MICAS mock-up is to study the free surface flow. Indeed numerical simulations cannot be performed in big geometries with such complex phenomena due to the too long calculation time. The use of a gas entrainment criterion is a way to address this issue. A criterion only based on local fluid properties and velocity can be calculated at each time step without slowing down the numerical code running. The Burger vortex model is used to build a gas entrainment criterion and the theoretical value was determined by assuming that a vortex carries gas when its depth gets over the distance between the outlet and the water surface. Velocity measurements were carried out in the MICAS mock-up to check the validity of this criterion in the upper plenum geometry. The PIV imaging technic was employed to measure the surface flow velocity around the vortex with different behaviours regarding the gas entrainment. The Burger model parameters versus the vortex state were calculated using the velocity results to build an experimental database. Regarding the Burger parameters, it seems that the downward velocity plays a minor role on the gas entrainment compared to the circulation. Finally, an experimental criterion was determined and compare to the theoretical one; the experimental value is

50 times smaller than the theoretical one. It may be due to the specific MICAS geometry or to the fact that the turbulence is neglected in the model.

REFERENCES

1. "4TH-Generation Sodium-Cooled Fast Reactors - The Astrid Technological Demonstrator", http://www.cea.fr/content/download/131897/2449556/file/4th-generation-sodium-cooled-fast-reactors.pdf (2012).

2. P. Le Coz, J.-F. Sauvage and J.-P. Serpantie, "Sodium-Cooled Fast Reactors: the ASTRID Plant Project", *Proceeding of ICAPP 2011*, Nice, France, 2-6 May, (2011).

3. P. Lo Pinto et al., "The Safety orientations during ASTRID conceptual design phase", *Proceeding of FR13, Paper CN-199-267, IAEA CN-199*, Paris, France, (2013).

4. F. Varaine, P. Marsault, M-S. Chenaud, B. Bernardin, A. Conti, P. Sciora, C. Venard, B. Fontaine, N. Devictor, L. Martin, "Pre-conceptual design study of ASTRID core", *Proceeding of ICAPP '12*, Chicago, United States, 24-28 Jun (2012).

5. J. Kremser, A. Lacroix, "Some Aspects of Sodium Technology Issued from the Operating Experience of RAPSODIE and PHENIX", *Proceedings of the international conference on liquid metal technology in energy production*, Champion, Pennsylvania, May 3–6, 1976.

6. G. Rodriguez et al., "Development of experimental facility platform in support of the ASTRID program", *Proceeding of FR13, Paper CN-199-122, IAEA CN-199*, Paris, France (2013).

7. O. Gastaldi et al., "Experimental platforms in support of the ASTRID program: Main experimental needs and devoted existing or planned facilities", *Proceeding of ICAPP 2015, Paper 15126, SFEN*, Nice, France (2015).

8. D. Guenadou, I. Tkatshenko and P. Aubert, "Plateau Facility in Support to Astrid and the SFR Program: an Overview of the First Mock-Up of the Astrid Upper Plenum, Micas", *Proceedings of NURETH16*, Chicago, Illinois, August 30–Sept. 4, 2015, pp. 5861-5872 (2015).

9. D. Guenadou, P. Aubert, V. Biscay, M. Bottin, J-P. Descamps, "Study of the Free Surface Flow in the MICAS Mock-Up in Support of the ASTRID SFR Program", *Proceedings of The 11th International Topical Meeting on Nuclear Reactor Thermal Hydraulics, Operation and Safety (NUTHOS-11)*, Gyeongju, Korea, October 9-13, 2016.

10. D. Tenchine, "Some Thermal Hydraulic Challenges in Sodium Cooled Fast Reactors", *Nuclear Engineering and Design,* **240**, pp. 1195-1217 (2010).

11. D. Tenchine, C. Fournier, Y. Dolias, "Gas entrainment issues in sodium cooled fast reactors", *Nuclear Engineering and Design,* **270**, pp. 302-311 (2014).

12. N. Kimura, T. Ezure, A. Tobita, H. Kamide, "Experimental Study on Gas Entrainment at Free Surface in Reactor Vessel of a Compact Sodium-Cooled Fast Reactor", *Journal of Nuclear Science and Technology,* **45**(10), pp. 1053-1062 (2008).

13. G Caruso, L Cristofano, M Nobili, D Vitale Di Maio, "Experimental Investigation of Free Surface Vortices and Definition of Gas Entrainment Occurrence Maps", 31st UIT (Italian Union of Thermo-fluid-dynamics) Heat Transfer Conference, Como, Italy, June 25–27, 2013.

14. T. Ezure , N. Kimura , K. Hayashi, H. Kamide, "Transient Behavior of Gas Entrainment Caused by Surface Vortex", *Heat Transfer Engineering*, **29**(8), pp. 659-666 (2008).

15. A.W. Patwardhan, R.G. Mali, S.B. Jadhao, K.D. Bhor, G. Padmakumar, G. Vaidyanathan, "Argon Entrainment into Liquid Sodium in Fast Breeder Reactor", *Nuclear Engineering an d Design*, **249**, pp 204-211 (2012).

16. B. Moudjed, J. Excoffon, R. Riva and L. Rossi, "Experimental Study of Gas Entrainment from Surface Swirl", *Nuclear Engineering and Design*, **310**, pp 351-362 (2016)

17. T. Sakai, Y. Eguci, H. Monji, K. Ito, H. Ohshima, "Proposal of Design Criteria for Gas Entrainment from Vortex Dimples Based on Computational Fluid Dynamics Method", *Heat Transfer Engineering*, **29**(8), pp 731-739 (2008).

18. J-M. Burgers, "A mathematical model illustrating the theory of turbulence", Advances in Applied Mechanics, **1**, pp. 171-199, (1948).